Coastal Circulation Caused by an Isolated Storm

J. A. CARTON[1]

Geophysical Fluid Dynamics Program, Princeton University, Princeton, NJ 08540

(Manuscript received 29 April 1983, in final form 15 August 1983)

ABSTRACT

The strength of storm generated coastal current and the intensity of coastal upwelling depend on the scales of the storm and the position of the storm with respect to the position of measurement. It is known that long coastal trapped waves travel poleward along eastern ocean boundaries and that a storm may generate these waves at its equatorward and poleward edges. If a storm lasts longer than coastal trapped waves take to propagate from the equatorward edge of the storm to the position of measurement, then the strongest current and upwelling occur poleward of the storm. If the storm is brief in this sense, then the strongest current and upwelling appear within the storm region after the storm decays.

A single storm with equatorward winds will generate a poleward traveling upwelling event followed by a more slowly traveling undercurrent event. The alongshore scale and time scale of the upwelling event bear a strong correspondence to the scales of the storm only if the storm starts and stops abruptly and has distinct edges in the alongshore direction. Continental shelf topography and friction alter the circulation quantitatively but not qualitatively.

1. Introduction

Winds blowing along the west coast of a continent towards the equator cause upwelling locally by driving near surface water offshore. An example of this is shown in Fig. 1 on 10–15 July. Southward winds cause a southward current and upwelling to develop. Upwelling, however, may also occur because winds further towards the equator have caused upwelling locally, which then spreads poleward along the coast in the form of coastal trapped waves. In Fig. 1 an event (actually downwelling) occurs on 31 July without any local strengthening of the wind field.

Models of coastal circulation may be roughly divided into those which depend only on the local winds, such as Allen (1973), Pedlosky (1978) and Hamilton and Rattray (1978), and those which depend on the remote alongshore winds as well, such as Gill and Clarke (1974), Gill and Schuman (1974), Csanady (1978), and Suginohara (1982). A number of studies, for example, Allen (1976), Chao (1981), and Yoon and Philander (1982) have explored the response of the second kind of model to particular idealized winds. In those studies the winds either remain steady in time after they begin or they are periodic. Similarly the winds are either constant in some bands of latitudes or are cyclic along the coast. However, taking the coastal region of Oregon as an example (cf. Fig. 1) actual winds are better described as a series of independent storms lasting a few days to weeks and stretching for hundreds of kilometers along the coast. These storms occur at random locations along the coast and are aperiodic in time.

In this paper we study the response of model coastal oceans to a single isolated storm in order to predict the amplitude and phase of the current and upwelling, given the space and time scales of the storm which generated them. The wind stress has the form $\tau = [0, \tau^y(y, t)]$. We think the actual winds are better described by a series of isolated storms of this kind than by the idealized winds previously considered.

We initially consider a reduced gravity ocean in which a single layer of uniformly light water overlies a much deeper layer of heavier water. Four examples of wind forcing are applied to this ocean in Section 2 to illustrate the effect that changes in the wind field have on the response. In the first example the wind is constant in the alongshore direction. In the second the wind decays toward the equator and is initiated at $t = 0$. The third example has winds which are confined to a band of latitudes, but are uniform within that band during a certain time interval and zero before and after (called top-hat forcing). The fourth example has Gaussian shaped winds which peak at one position alongshore, and decay gradually in both directions and peak at one moment in time, and build up and decay gradually with time. In the third section we introduce a continuously stratified ocean model and compare its response to Gaussian winds for several stratification profiles. In the fourth section continental shelf topography and friction are introduced.

[1] Present affiliation: Center for Earth and Planetary Physics, Harvard University, Cambridge, MA 02138.

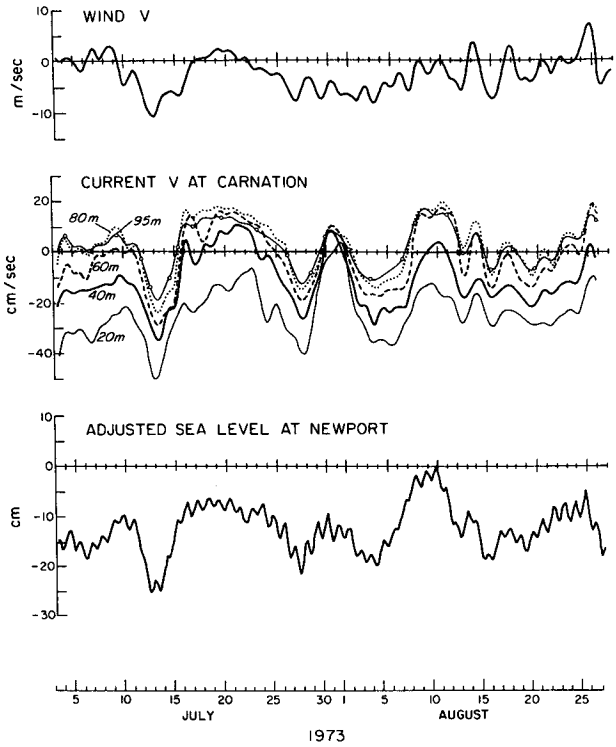

FIG. 1. Alongshore wind, current, and sea level for 3 July–27 August 1973 (from Kundu *et al.*, 1975). The current was measured at 45°16′N on the 100 m isobath. Wind and sea level were measured at Newport, Oregon (44°40′N).

2. The response of a reduced gravity ocean

The first coastal ocean model we would like to consider is one which has linear, hydrostatic, inviscid motion in one layer of water bounded below by a deep motionless second layer. A one active layer (reduced gravity) model is a reasonable model to choose because we anticipate that the flow in an actual coastal ocean will be concentrated near the surface. The change in density between the two layers of our model is small ($\Delta\rho/\rho \ll 1$) and the surface stress is assumed to be uniformly distributed over the upper layer. A wall exists to the east, at $x = 0$, and the ocean extends to negative x. Charney (1955) provides a derivation of a somewhat more general model. The zonal acceleration term is neglected here, following the results of Gill and Clarke (1974), since we are only interested in the dynamics of the near shore water at time scales longer than the inertial time scale. The equations of motion reduce to

$$-fV = -P_x, \tag{2.1a}$$

$$V_t + fU = -P_y + \frac{\tau^y}{(\rho H)}, \tag{2.1b}$$

$$P_t + C^2(U_x + V_y) = 0, \tag{2.1c}$$

where the interface height $\eta = -P\rho/(g\Delta\rho)$, $C = (gH\Delta\rho/\rho)^{1/2}$ is the speed of internal waves in the irrotational system, f the Coriolis term and U and V are the eastward and northward velocities. For the calculations in this section, $C = 1.22$ m s^{-1}. The height H is taken to be 107 m; this choice is not important, as H only affects the relative amplitude of the response. Upwelling in this simple model occurs when the interface height is raised above its quiescent value.

If the forcing is an alongshore wind stress independent of x then Gill and Clarke show that the Eq. (2.1) may be reduced to an equation for ξ

$$\xi_t + C\xi_y = \tau(y, t), \tag{2.2}$$

where

$$\left.\begin{aligned} \tau &= \tau^y(y, t/(\rho H) \\ U &= -\tau(y, t)(\exp(x/\lambda) - 1)/f \\ V &= \xi(y, t)\exp(x/\lambda) \\ P &= C\xi(y, t)\exp(x/\lambda) \end{aligned}\right\}, \tag{2.3}$$

and $\lambda = C/f$ is the radius of deformation. Eq. (2.2) has a homogeneous solution which is a Kelvin wave trapped within a radius of deformation of the coastline. The Kelvin wave propagates poleward along eastern boundaries with speed C.

A general solution to (2.2), was obtained by Gill and Clarke (1974) and Gill and Schumann (1974) using the method of characteristics. In this method the solution is expressed at some point in space y and time t as an integral of the contributions of the forcing at all previous times t_i, which could affect the solution at time t. Expressed mathematically, the solution becomes

$$\xi(y, t) = \int_{-\infty}^{t} \tau(C(t_i - t) + y, t_i)dt_i. \tag{2.4}$$

To illustrate the properties of equation (2.2), we solve (2.4) with four forms of alongshore wind stress forcing.

Example 1. The alongshore stress in the first example is independent of alongshore direction; it begins to blow towards the equator at $t = 0$ and then remains constant. Eq. (2.4) reduces to $\xi(t) = t\tau$. The alongshore current and upwelling intensify linearly in time, as shown in Fig. 2a. This is a special case of the two layer problem considered by Charney (1955). Suppose the wind is turned off at $t = T_0$. Then the current and upwelling persist at later times because the current is in geostrophic balance in the offshore direction with the pressure field.

Example 2. The wind blows equatorward with constant force over a finite band of latitudes, $0 < y < Y_0$, after being turned on at $t = 0$. This problem is discussed by Allen (1976). Initially the current in the region of forcing behaves as in Example 1, increasing linearly in time. After time y/C an alongshore pressure gradient

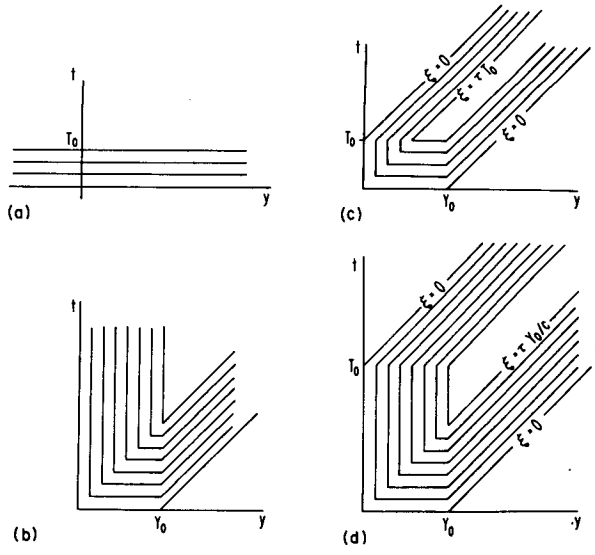

FIG. 2. Alongshore velocity in the y–t plane for three types of equatorward stress. Constant phase lines of Kelvin waves intersect the y axis at an angle of 45°. (a) Wind stress which is independent of y, turns on at $t = 0$ and turns off at $t = T_0$. (b) Wind stress which is confined alongshore between 0 and Y_0, and turns on at $t = 0$. (c) Wind stress which is top-hat shaped, confined in space and time with scales Y_0 and T_0 where $CT_0/Y_0 < 1$. (d) Wind stress which is top-hat shaped with $CT_0/Y_0 > 1$.

develops in the wake of a wave generated at the equatorward edge of the region of forcing. The pressure gradient balances the wind stress and so the current and upwelling become steady (Fig. 2b).

Poleward of the forcing region the current and upwelling begin to accelerate in the wake of a Kelvin wave generated at the poleward edge of the forcing region and they stop accelerating when a Kelvin wave arrives from the equatorward edge, setting up an alongshore pressure gradient.

Example 3. The wind is shaped like a "top hat" in time and alongshore direction:

$$\tau^y = \begin{cases} -1.0 \text{ dyn cm}^{-2}, 0 \leq t \leq T_0, & 0 \leq y \leq Y_0 \\ 0, \quad \text{otherwise.} \end{cases}$$

Within the forcing region, while the wind is blowing, the ocean acts as it did in Example 2. For $t < y/C$ the current and upwelling intensify and for longer times they are steady. The behavior of the ocean after the wind has stopped, poleward the forcing region, depends on the parameter $\epsilon \equiv CT_0/Y_0$ which is the ratio of the time scale T_0 to the adjustment time Y_0/C.

In Example 1 a current persists after the wind stops blowing. That is possible here too, provided the storm is sufficiently brief ($\epsilon < 1$). For brief storms the most intense current and upwelling in the forcing region occurs after the storm decays. The presence of an equatorward edge to the forcing becomes important at $t = y/C$. At later times the current and upwelling decay.

For long lasting storms ($\epsilon > 1$) a Kelvin wave from the equatorward edge of the forcing region propagates completely across the forcing region, while the wind is blowing. The most intense current and upwelling occur at the poleward edge after the arrival of the Kelvin wave but while the wind is still blowing.

Poleward of the forcing region, four waves become important. For brief storms ($\epsilon < 1$) the current intensifies linearly beginning at $(y - Y_0)/C$ in the wake of a Kelvin wave arriving from the poleward edge of the region of forcing at the beginning of the storm (Fig. 2c). At $t = T_0 + (y - Y_0)/C$ the flow becomes steady in the wake of a Kelvin wave arriving from the poleward edge of the forcing region, announcing the end of the storm. The current begins to decay at $t = y/C$ when a wave arrives which was generated at the equatorward edge of the forcing region at the beginning of the storm. By $t = T_0 + y/C$ the current is zero and the upwelling has stopped, corresponding to the arrival of a Kelvin wave from the equatorward edge of the forcing region at the end of the storm.

For long lasting storms ($\epsilon > 1$), poleward of the forcing region, the acceleration also starts with the arrival of a wave from the poleward edge of the forcing region at the beginning of the storm. However the next wave to arrive is a wave generated at the equatorward edge of the forcing region at the beginning of the storm. This wave sets up an alongshore pressure gradient, halting the acceleration of the current a time interval Y_0/C after the current began. The current is steady until $t = T_0 + (y - Y_0)/C$, when a Kelvin wave arrives from the poleward edge of the forcing region at the end of the storm causing the flow to weaken.

At a position poleward of the forcing region, the length of time for which the alongshore current is most intense is given by the absolute value of the difference between the time scale of the forcing and the adjustment time scale, $|(\epsilon - 1)Y_0/C|$. For brief storms ($\epsilon < 1$) the time scale of the maximum response may be quite long compared to the time scale of the forcing. This is because the waves must arrive from the equatorward edge of the forcing region in order to cause the current to decay. For long lasting storms ($\epsilon > 1$) the time scale of the maximum response is also long. If $\epsilon \sim 1$ the response is either growing or decaying but does not linger at its maximum value.

The length of time from when the current first begins until it ends is $T_0 + Y_0/C$ when measured poleward of the forcing region. Half the difference between the time-span of the complete response and the maximum response gives a value for the rise time of the current pulse. For $\epsilon < 1$ the rise time is T_0, but for $\epsilon > 1$ the rise time is Y_0/C.

If the storm propagates significantly in the alongshore direction or is asymmetric, for example growing gradually in the south but suddenly in the north, then

the rise time and the decay time may be quite different and these results no longer hold.

Poleward of the region of forcing for stationary storms, if we know whether ϵ is greater than or less than one and if the shape of the storm is approximately that considered here, we may deduce both T_0 and Y_0. The upwelling event generated by a given storm may be nearly precisely identified.

Example 4. The response to Gaussian forcing of the form

$$\frac{\tau^y(y, t)}{(\rho H)} = \tau \exp\left[-\left(\frac{2y}{Y_0}\right)^2 - \left(\frac{2t}{T_0}\right)^2\right], \quad (2.5)$$

is considered, now where the maximum stress, $\tau(\rho H)$, is -1.0 dyn cm^{-2}. Substituting (2.5) into (2.4) gives

$$\xi = \frac{CT_0\tau\sqrt{\pi}}{4}\left[\operatorname{erf}\left\{\frac{2\epsilon\hat{y} + 2\hat{t}/\epsilon}{(\epsilon^2 + 1)^{1/2}}\right\} + 1\right] \times \exp\left[\frac{-4(\hat{t} - \hat{y})^2}{(\epsilon^2 + 1)}\right], \quad (2.6)$$

where $\hat{t} = Ct/Y_0$, $\hat{y} = y/Y_0$, $\epsilon = CT_0/Y_0$.

For very brief ($\epsilon \ll 1$) or for very long lasting storms ($\epsilon \gg 1$) the response is qualitatively similar to that of the top-hat forcing case. For very brief storms the current in the region of forcing continues to intensify as long as the wind is blowing, and so the maximum current occurs as the wind decays (Fig. 3a). For very long lasting storms the maximum response is shifted poleward from the position of maximum winds but occurs before the storm has ended (Fig. 3b). However if the storm is such that $\epsilon \sim 1$, then both time delays and shifts in space of the maximum response occur.

With top-hat shaped forcing the time and space scales of the forcing could be reduced to two possibilities given measurements of the response poleward of the region of forcing. When the forcing is Gaussian-shaped the duration of the response poleward of the region of forcing is $Y_0[C^2(\epsilon^2 + 1)]^{-1/2}$. If the storm which generated the event was very brief ($\epsilon \ll 1$) then the response lasts for a time Y_0/C. If the storm was long lasting ($\epsilon \gg 1$) then the response lasts for a time T_0. In these two limits the storm length or time scale may still be deduced. The other scale can be determined from simultaneous alongshore measurements. But if the storm is neither very brief nor very long lasting ($\epsilon \sim 1$) then the storm scales may not be deduced. This inability occurs because of the smoothly growing and decaying nature of the Gaussian. The Gaussian forcing shape is more representative of real storms than the top-hat forcing, so it will be used in the subsequent calculations.

In this section and Section 3 the time scale rather than the length scale of the forcing is varied. However, for forcing which depends only on t/T_0 and y/Y_0, the results for varying the length scale $Y_0 \rightarrow Y_0/\alpha$ may be obtained by the transformation

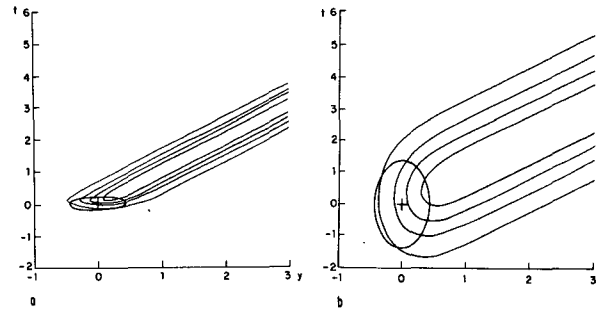

FIG. 3. As in Fig. 2 with Gaussian-shaped forcing. The scales are (a) T_0 = 3 days, y_0 = 1000 km; (b) T_0 = 30 days, Y_0 = 1000 km. Time is marked in tens of days. The contour intervals are (a) 3 cm s^{-1} and (b) 30 cm s^{-1}.

$$T_0 \rightarrow T_0\alpha, \quad t \rightarrow t/\alpha, \quad y \rightarrow y/\alpha.$$

Halving the length scale of the storm is equivalent to doubling its time scale and halving the scale of the time and the alongshore distance axes. As we shall see, however, this correspondence does not occur when continental shelves are present and the alongshore scale of the storm is small. This problem will be raised in Section 4.

3. Response of a stratified ocean with a flat bottom

To study the vertical structure of coastal upwelling we must use a more sophisticated ocean model than the reduced gravity model since all motion in that model is confined to a single layer. The model we choose is that of a continuously stratified ocean. In such an ocean the availability of many modes with differing vertical structure means that a coastal undercurrent may be established below the directly wind forced layer. Yoon and Philander (1982) describe the evolution of the currents after the sudden onset of an alongshore wind. McCreary (1981) describes the steady state current when a particular form of vertical dissipation is present.

Here we consider the response of a continuously stratified ocean to Gaussian forcing, which differs from the forcing used in these earlier studies in that its wind is transient. The model is linear, hydrostatic, inviscid and contains no continental shelf. The wind stress is represented by a body force in a surface layer of depth H = 20 m. The equation of motion are (Gill and Clarke, 1974)

$$U_t - fV = -P_x/\rho_0, \quad (3.1a)$$

$$V_t + fU = -P_y/\rho_0 + \tau^y/(\rho_0 H), \quad (3.1b)$$

$$U_x + V_y + W_z = 0, \quad (3.1c)$$

$$\frac{P_{zt}}{\rho_0} + N^2 W = 0, \quad (3.1d)$$

where

$$N(z) = \left(\frac{-g\partial\rho(z)/\partial z}{\rho_0}\right)^{1/2}$$

is the Brunt–Väisälä frequency. The vertical dependence of these equations is separated out following the procedure of Gill and Clarke. Expand

$$U = \sum_{n=0}^{\infty} U_n(x, y, t)\phi_n(z), \quad V = \sum_{n=0}^{\infty} V_n(x, y, t)\phi_n(z),$$

$$P = \sum_{n=0}^{\infty} P_n(x, y, t)\phi_n(z), \quad W = \sum_{n=0}^{\infty} W_n(x, y, t)\bar{W}_n(z),$$

$$\tau^y = \sum_{n=0}^{\infty} \tau_n(y, t)\phi_n(z), \tag{3.2}$$

where

$$\phi_n(z) = d\bar{W}_n/dz, \tag{3.3}$$

$$d^2\bar{W}_n/dz^2 + \frac{N^2}{C_n^2}\bar{W}_n = 0 \tag{3.4}$$

with boundary conditions $\bar{W}_n = 0$ at $z = (D, 0)$ where $-D = 2000$ m is the bottom. The upper boundary condition on $\bar{W}$ eliminates the barotropic response, which should be small because of the high speed of barotropic waves, typically $C_0 \sim 200$ m s^{-1}. The equations describing the horizontal evolution of each mode are then the same as (2.2) and (2.3). The upper limits of the summations in (3.2) are taken to be 15. The higher modes are important only within a kilometer or so of the coast (see Yoon and Philander, 1982). The standard stratification, shown in Fig. 4a, is the same as that used by Yoon and Philander. In addition two other stratifications are shown which will be discussed later. The vertical structure functions $\phi_n(z)$ were obtained by solving (3.4) using a shooting method in which the values C_n were chosen to satisfy the boundary conditions on W_n. The first three vertical structure functions for the standard stratification are shown in Fig. 4b.

Dependence on the time scale of the storm. Gaussian shaped storms lasting $T_0 = 3$, 12 and 30 days are compared here. The parameter $\epsilon_1 = C_1T_0/Y_0$ for these storms has values 0.32, 1.2, and 3.2. The alongshore velocity in Fig. 5a is initially in the direction of the wind but lags by several days. The current pulse appears to propagate faster than the free wave speed in the vicinity of the storm. In these respects the continuously stratified ocean resembles the reduced gravity ocean. But the maximum velocity in the continuously stratified ocean occurs poleward of the region of forcing, rather than within the region of forcing as was the case for brief storms in a reduced gravity ocean. This happens because the different wave modes excited by the storm interfere with each other within the region of the storm but gradually separate because of their differing speeds as they propagate poleward.

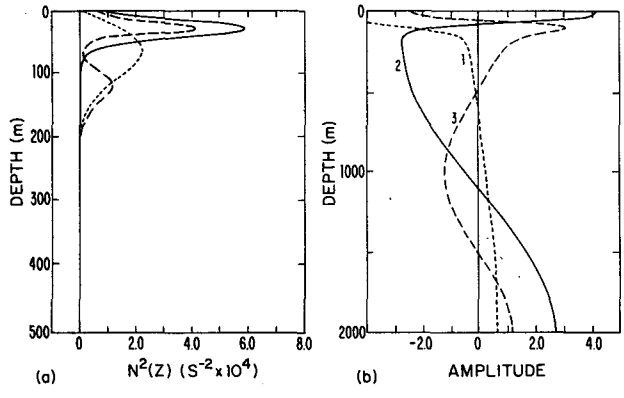

FIG. 4. Stratification as a function of depth for several different density profiles in (a). The standard stratification is marked with a short dashed line. The first three modes of the horizontal velocity field for the standard stratification are shown in (b).

As the time scale of the storm increases, the time at which the maximum current is observed within the forcing region approaches the time of maximum wind stress (compare Fig. 5a and Fig. 5c). Also the maximum current while the wind is blowing is shifted well poleward of the region of the storm.

Several authors have studied the development of an undercurrent by winds which vary in the alongshore direction. Yoon and Philander (1982) and Crepón and Richez (1982) point out that Kelvin waves generated at the equatorward edge of the region of forcing bring with them an alongshore pressure gradient, which in turn drives an undercurrent. A useful alternative explanation of this phenomenon is that an undercurrent occurs when various wave modes excited by the wind change their relative phases as they travel poleward, because of the differences in their speeds. For example, in Fig. 5a an undercurrent develops after the storm has died, as the first baroclinic wave outruns the higher baroclinic waves. This undercurrent appears to travel initially at an anomalously rapid speed, as the result of interference between different waves. The initial pulse of current extends far offshore. Following it more slowly is a pulse of undercurrent which is more closely confined to the coast (Fig. 6).

The summer waters near the coast of Oregon have a sharp thermocline in the upper 10–30 m (Mooers *et al.*, 1976) and a deeper permanent pycnocline at 100–200 m. This density structure changes seasonally. McCreary (1981) found that the steady response of a stratified ocean was insensitive to changes in stratification. To determine what effect a shallow thermocline has on the storm generated currents we also study the response with a mean stratification profile which peaks sharply at 30 m depth and a stratification profile which has both a thermocline at 30 m and a deeper permanent pycnocline at 120 m. These curves are shown in Fig. 4a. The total 0 to 2000 m temperature contrast is the same in each case.

The forcing considered here has scales $T_0 = 3$ days, $y_0 = 1000$ km and $\epsilon_1 = 0.24$ for the shallow thermocline, and $\epsilon = 0.31$ for the double pycnocline case. Offshore-vertical profiles of current for the three strat-

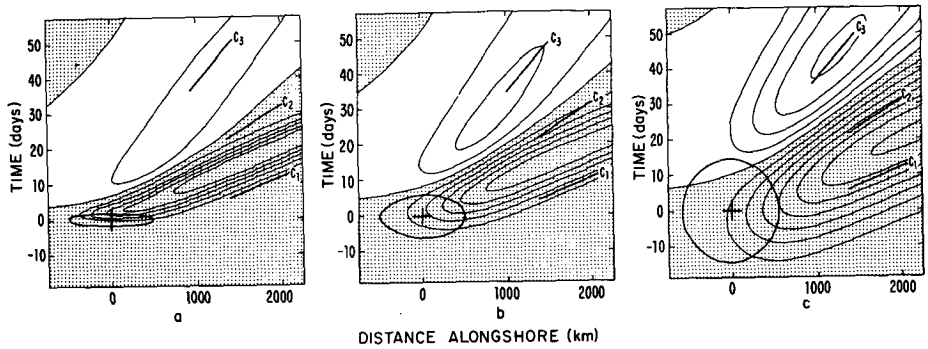

FIG. 5. Alongshore velocity in the y–t plane for the continuously stratified ocean model with vertical coasts. Measurements are at a depth of 75 m, 7 km from the coast. Constant phase lines of the first three wave modes are shown. An ellipse marks the alongshore forcing region and the time span of the forcing. The time scales of forcing are (a) 3, (b) 12 and (c) 30 days. Contour intervals are 2, 5 and 5 cm s^{-1}. Shaded regions are negative.

ifications are shown in Fig. 7. The cross sections are taken at y = 1000 km and t = 6 days. By this time the first mode has arrived from the region of forcing, so that the lefthand panel of Fig. 7 has the structure of the first mode. By t = 12 days the higher baroclinic modes have arrived and an undercurrent develops. The second stratification, however, generates a weak undercurrent since the first baroclinic mode is concentrated within the depth of the mixed layer (20 m). Qualitatively however, the undercurrent does not appear to be sensitive to the stratification.

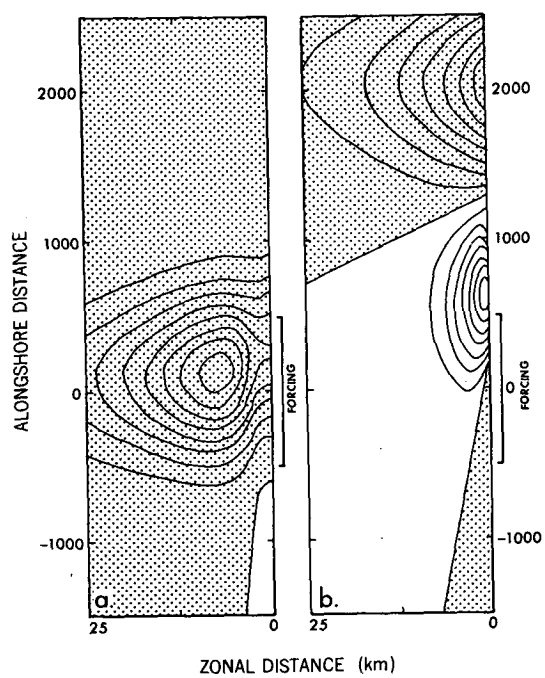

FIG. 6. Alongshore velocity in the x–y plane at 70 m depth. Plots are snapshot views at (a) t = 0 and (b) t = 12 days. Forcing is Gaussian-shaped with y_0 = 1000 km, T_0 = 3 days and standard stratification. Contour intervals are 0.25 and 2.5 cm s^{-1}. Shaded regions are negative.

4. Continental shelf

When a continental shelf is included in the coastal ocean, internal Kelvin waves are replaced by a hybrid form of stratified coastal trapped waves. These waves may resemble Kelvin waves or barotropic shelf waves depending on the ratio of the radius of deformation to the shelf width (Huthnance, 1978). For a radius of deformation of 12 km and the shelf considered here this ratio is about ⅓ (typical of the waters off Oregon) so that the coastal trapped waves are strongly influenced by topography. In this section we treat the influence that shelf topography has on the response of a coastal area to a storm. The shelf topography consists of an upper shelf and a steeper shelf slope, both varying linearly with longitude (with the coast at $\lambda = 0°$):

$$D(\lambda) = \begin{cases} -40 + 400\lambda \text{ m}, & -0.4° \leqslant \lambda \leqslant 0 \\ -200 + 19\,800(\lambda + 4°) \text{ m}, & \\ \qquad\qquad -1.28° \leqslant \lambda \leqslant -0.4° & \\ -2000 \text{ m}, \quad \lambda \leqslant -1.28°. & \end{cases} \tag{4.1}$$

The vertical dependence of the response when a continental shelf is included may no longer be separated from the dependence on the offshore coordinate, so wave modes have been computed by resonance iteration of an offshore-vertical, f-plane gridpoint model. The basic equations are again given by (3.1a)–(3.1d). The horizontal resolution is 7.5 km. Seventeen gridpoints are distributed uniformly in the vertical at each horizontal grid position.

Evaluated at 45°N with a 1000 km alongshore wavelength, the first mode is nearly depth independent with most of the flow confined to the upper shelf (Fig. 8). The second wave mode shows some bottom trapping on the shelf slope and the third wave mode, which is not shown here, has some bottom trapping on the upper shelf. The alongshore speeds of the first three

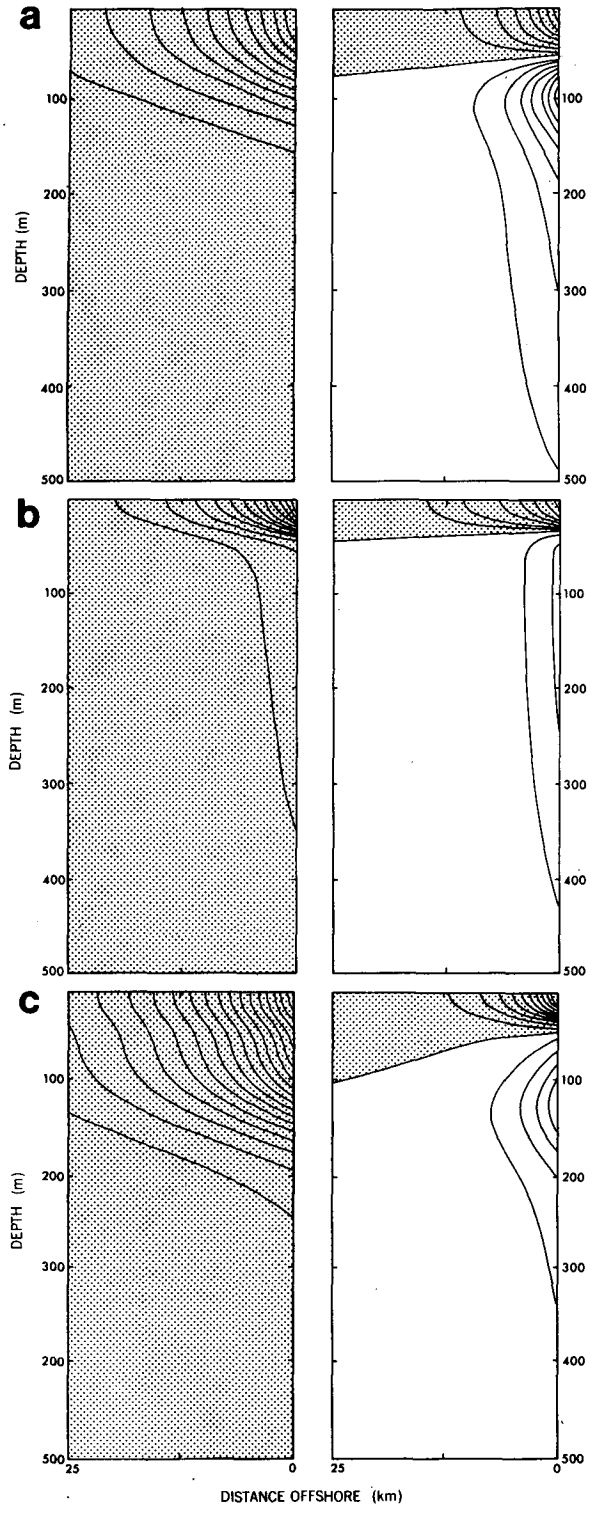

FIG. 7. Alongshore velocity in the x–z plane for the three stratifications shown in Fig. 4a. The left-hand plots were made at $t = 6$ days, $y = 1000$ km, during the passage of the first mode wave from the storm region. The right-hand plots were made at $t = 12$ days, $y = 1000$ km. The forcing in each case is Gaussian with $Y_0 = 1000$ km, $T_0 = 3$ days, centered at $y = 0$, $t = 0$. Contour intervals in (a) with the standard stratification, are 2.5 cm s^{-1} for the left-hand plot and 1.0 cm s^{-1} for the right-hand plot, in (b) for the near surface pycnocline are 2.5 and 1.0 cm s^{-1}, and in (c) for the two pycnocline stratification are 2.5 cm s^{-1}. Shaded regions are negative.

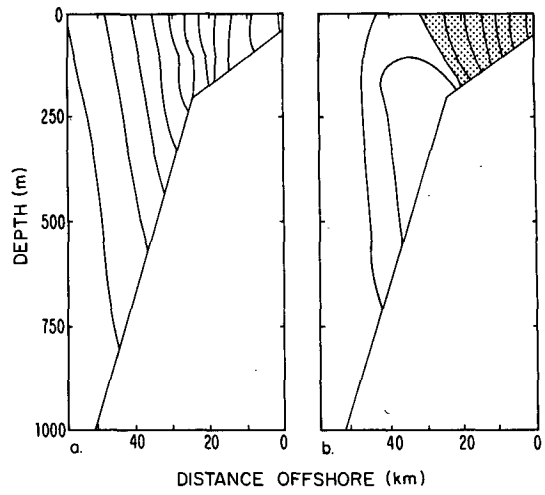

FIG. 8. First two meridional velocity wave modes at 45°N in the x–y plane for an ocean with the standard stratification and shelf topography. The alongshore wavelength of both waves are chosen to be 1000 km. The second wave mode shows some bottom trapping.

wave modes are 3.8, 0.9 and 0.6 m s^{-1}. The pressure modes are no longer proportional to the alongshore velocity modes since the offshore behavior of the modes [cf. (2.3)] is no longer constrained to behave exponentially.

The presence of a pycnocline at 120 m in stratification number 3 causes the first mode alongshore velocity field to spread off the upper shelf. The speed of the first mode increases while the second mode slows slightly. A similar effect is discussed by Huthnance (1978) as the stratification becomes more vertically distributed.

Response of a stratified ocean with a continental shelf. Suginohara (1982) considered the response of a stratified ocean with shelf topography to winds turned on at $t = 0$. He found that coastal trapped waves replace Kelvin waves in halting the acceleration of the alongshore velocity and upwelling. In the wake of coastal trapped waves generated at the equatorward edge of the wind, upwelling is balanced by convergence of alongshore transport as well as by convergence of the onshore transport.

Here we consider a wind event confined both in space and time in the form of a Gaussian distribution applied to a coastal ocean with stratification and topography. We could proceed, as we do in the absence of the continental shelf, by summing up coastal trapped wave modes with amplitudes and phases chosen to satisfy the forced problem. However, we choose instead to use a multilevel ocean model with topography defined by (4.1) which contains the additional effects of

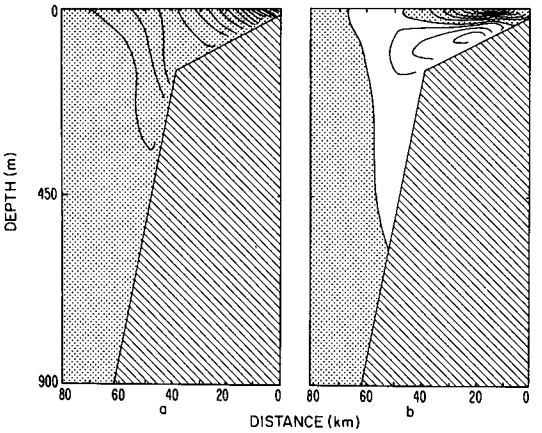

FIG. 9. Alongshore velocity in the x–z plane at 35°N from the multilevel model. The forcing is Gaussian with scales T_0 = 3 days, Y_0 = 1100 km, and $\tau^y(35°, 0) = -1.0$ dyn cm^{-2} centered at 35°N. The plots were made at (a) $t = 0$ and (b) $t = 6$ days. Contour intervals are 1.0 and 0.5 cm s^{-1}. Shaded regions are negative.

the variation of the Coriolis parameter with latitude, friction, diffusion, and nonlinearity. The coastal trapped wave modes discussed before are used in the analysis of the ocean model results. A description of the multilevel model is provided in the Appendix.

The wind stress at maximum strength is -1.0 dyn cm^{-2} with time scale and length scale T_0 = 3 days and Y_0 = 1100 km, yielding $\epsilon_1 = 0.98$. The model is run for 15 days beginning at day -3. The flow at $t = 0$ days (Fig. 9a) at the center of the region of forcing is fairly depth independent with a structure similar to the first baroclinic mode. The greatest velocity is 17 cm s^{-1}. Water is transported offshore in the surface Ekman layer and is replaced partly by inflow along the bottom Ekman layer but mainly by convergence of water in the alongshore direction. By $t = 2T_0$, long after the storm has ended, the flow in the forcing region is weak and has developed an undercurrent on the upper shelf with maximum velocity of 2.0 cm s^{-1}. The undercurrent surfaces offshore. The pulse of southward current propagates poleward causing upwelling as it propagates due to dissipation of the wave in the bottom boundary layer and the convergences of water within the pulse.

In the upper layers the alongshore velocity is greatest in the forcing region but decays as the modes separate (Fig. 10b). At 175 m, however, the maximum velocity occurs after the modes have separated, poleward of the forcing region (Fig. 10a). The deep thermal anomaly is nearly in phase with the alongshore velocity. In order to determine the influence of friction on the response, the calculation was repeated, once with a free slip condition on the bottom and once with a constant vertical viscosity of 1.0 cm^2 s^{-1}. In each case the qualitative results were the same. For the intensity of wind stress we consider here, Philander and Yoon (1982) find the nonlinear terms are relatively unimportant.

When the alongshore length of the storm decreases, the ratio of the storm duration to the adjustment time scale ϵ increases, and we expect from Section 3 that the amplitude of the response decreases. An alongshore–time plot of alongshore velocity for forcing scales Y_0 = 110 km, T_0 = 3 days is shown in Fig. 11. The wind in this case was northward (τ^y = 1.0 dyn cm^{-2}). The undercurrent is much stronger relative to the surface current for the case of small alongshore scale winds. There are two reasons for this:

1) As the scale of the forcing approaches the scale width of the shelf all the coastal trapped waves become increasingly bottom trapped (as shown in Huthnance, 1978).

2) The first mode is relatively depth independent and travels more rapidly than the higher modes. For the scales given above, using speeds computed at 35°N for 100 km scale waves, $\epsilon_1 = 2.8 \times 3.0 \times 84\,400/110\,000 = 6.6$ while $\epsilon_2 = 1.8$ and $\epsilon_3 = 0.85$. This means

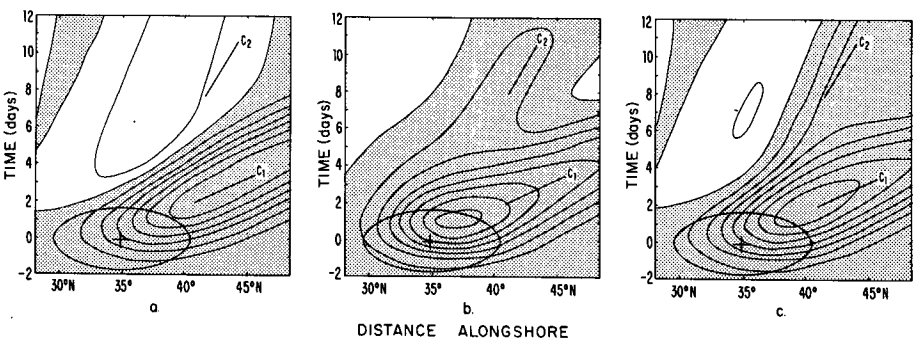

FIG. 10. Plots (Y–t) of alongshore velocity in (a) and (b), and temperature anomaly in (c). The depths and distances from the coast are (a) 175 m and 0.64°, (b) 50 m and 0.27°, and (c) 175 m and 0.64°. The scales of the forcing are Y_0 = 1100 km, T_0 = 3 days, $\tau^y(35°, 0) = -1.0$ dyn cm^{-2}. Lines of constant phase for the first two coastal wave modes are drawn. The contour intervals are 1.0, 0.5 cm s^{-1}, and 0.0025°C. Shaded regions are negative.

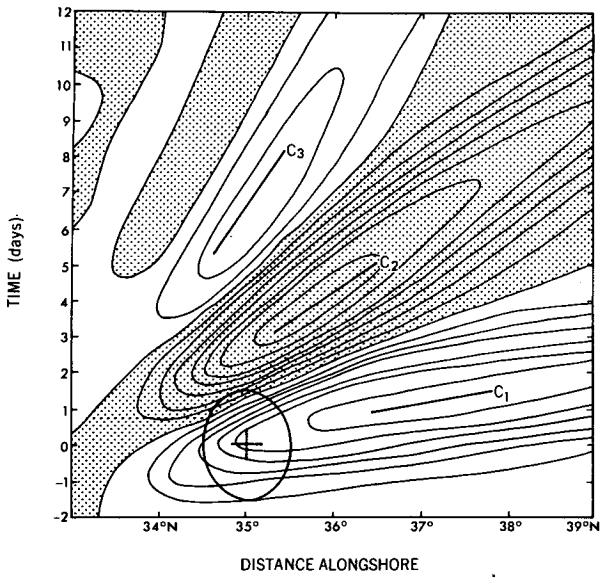

FIG. 11. Alongshore velocity in the y–t plane for Gaussian forcing with scales Y_0 = 110 km, T_0 = 3 days, and $\tau^y(35°, 0)$ = 1.0 dyn cm^{-2}. Measurements are at 175 m, 0.64° from the coast. The contour interval is 0.1 cm s^{-1}. Lines of constant phase for the first three coastal wave modes, computed at 35°N with 200 km wavelengths, are indicated. Note that the undercurrent is nearly as strong as the initial current. Shaded regions are negative.

that the relatively depth independent first mode has adjusted during the storm while the higher modes continue to intensify throughout the storm. The higher coastal trapped modes are more bottom trapped (Huthnance, 1978), and so as they become relatively more important the undercurrent becomes relatively more intense.

The relative weakness of the depth independent response comes about because the first few shelf waves rapidly cross the small forcing region, halting the growth of the alongshore current. This implies that, if most of the observed current with synoptic scales is composed of the first two shelf modes which are relatively depth independent, only alongshore scales in the wind field greater than C_2T_0 need be observed in order to predict the alongshore current field. Taking T_0 = 5 days and C_2 = 1 m s^{-1} this gives $C_2T_0 \approx 500$ km. At lower latitudes the speed of coastal trapped waves decreases as f decreases and so smaller scales in the wind may be important.

5. Discussion

In this paper we have considered the response of a hierarchy of coastal ocean models to a storm which is confined in the alongshore direction and in time. We make predictions about the strength and phase of currents and upwelling given the scales of the wind. The response of the reduced gravity ocean within the region of the storm along eastern boundaries depends on the ratio of the storm duration to the time a coastal trapped wave takes to propagate in to the position where the response is measured, from the edge of the storm closest to the equator. In our notation this ratio is $T_0/(L/C)$. When this ratio is much greater than one, when for example the storm is long-lasting, the maximum alongshore current and upwelling occur during the passage of the storm. When this ratio is much less than one the maximum alongshore current and upwelling occur after the passage of the storm.

Figure 1, taken from Kundu *et al.* (1975), shows the time history of the alongshore winds, current and surface elevation off the coast of Oregon during July and August 1973. The storm which begins on 10 July, lasts for five days while the largest current and upwelling occur a day or two before the end of the storm. This suggests that the storm lasted longer than waves took to travel from the edge of the storm closest to the equator, to the position where the measurements were made. If we assume that the storm is top-hat shaped then we can estimate the distance the storm extends towards the equator. Taking the speed of alongshore waves to be 4 m s^{-1} this distance is $\sim C\Delta t$ = 1200 km.

Poleward of the region of forcing, the strength of currents in the reduced gravity ocean depends on the ratio ϵ of the time scale of the storm to the time waves take to propagate alongshore through the whole alongshore extent of the storm, $T_0/(Y_0/C)$. The importance of this ratio was also noted by Allen (1980). For long-lasting, top-hat shaped storms ($\epsilon < 1$) growth or decay of the alongshore current occurs over a time Y_0/C. For brief storms ($\epsilon > 1$) the growth or decay occurs over the time the original storm lasted T_0. When the scales of the forcing are less distinct, as in the case of Gaussian shaped storms, these results only apply in the limits of $\epsilon \gg 1$ or $\epsilon \ll 1$.

In a continuously stratified ocean many coastal trapped waves are available with differing vertical structures. These waves allow currents and upwelling to vary with depth. The response of such an ocean to a Gaussian shaped storm is initially a fairly vertically independent flow in the direction of the wind followed by an undercurrent, flowing in the opposite direction. Returning to Fig. 1, after the storm of 10–15 July the current below the mixed layer flows in the opposite direction to the wind.

The undercurrent in a continuously stratified ocean travels poleward more slowly than the approximately vertically independent current. Thus instruments moored poleward of a storm in such an ocean would detect a pulse of current and upwelling in which the current would be in the direction of the wind followed by a longer lasting undercurrent pulse. Outside the region of forcing, these current pulses may be separated significantly in time. Could the current events of 31 July and 10 August shown in Fig. 1 have been caused

by the same storm? If the difference in speed between these two pulses were 2 m s^{-1} this would suggest that they were generated ~2000 km to the south.

Changes in the density of the ocean alter its response to storms by changing the vertical dependence and speeds of the coastal trapped waves. When, for example, the vertical structure of the first baroclinic wave becomes similar to the directly wind forced current, the undercurrent weakens. Continental shelf topography also alters the structure and speeds of coastal trapped waves. However, the results obtained neglecting the shelf appear still to apply qualitatively.

The storm and ocean models considered in this study are greatly simplified. For example, large scale winds which blow for many days are required in order to generate a strong coastal undercurrent in the model considered in this study. However, it is possible that variations in alongshore topography, neglected in this study, may be important sources of energy for waves which vary strongly in the vertical direction, necessary in order to generate a strong coastal undercurrent.

Coastal observation studies have concentrated on determining the cross-shelf and vertical structure of the coastal currents. For the simple models we have considered here, the response in the forced and free regions, that is, in different places alongshore, are quite different. In order to understand the connection between the local response and free waves in coastal ocean adjustment, contemporaneous measurements at many points alongshore need to be studied. These would identify both the region of forcing and the freely propagating response.

Acknowledgments. I thank George Philander for suggesting this study, and he, George Mellor, and Chris Mooers for reading earlier versions of this manuscript. John Allen provided Fig. 1 and Ken Brink provided the code used to compute the coastal trapped wave modes. Renate D'Arcangelo typed versions of this manuscript. Much of this work was done at the Geophysical Fluid Dynamics Program, Princeton University, supported by NOAA Grant 04-7-022044017. Harvard University has provided additional support under ONR Grant N00014-75-C-0225.

APPENDIX

Three-Dimensional Ocean Model

The model used here is a version of the GFDL three-dimensional ocean model. The equations of motion under the rigid-lid, Boussinesq and hydrostatic assumptions are

$$\left.\begin{aligned}
&\frac{\partial U}{\partial t} + L(U) - \frac{UV}{a}\tan\phi - fV = \frac{-1}{\rho_0 a\cos\phi}\frac{\partial P}{\partial\lambda} + \frac{\partial}{\partial z}\left(\frac{A_v}{\gamma}\frac{\partial U}{\partial z}\right) \\
&\qquad + A_m\left[\nabla^2 U + \frac{(1-\tan^2\phi)}{a^2}U - \frac{2\sin\phi}{a^2\cos^2}\frac{\partial V}{\partial\lambda}\right] + \frac{\partial\tau^x}{\partial z\rho_0} \\
&\frac{\partial V}{\partial t} + L(V) + \frac{U^2}{a}\tan\phi + fU = -\frac{1}{\rho_0 a}\frac{\partial P}{\partial\phi} + \frac{\partial}{\partial z}\left(\frac{A_v}{\gamma}\frac{\partial V}{\partial z}\right) \\
&\qquad + A_m\left[\nabla^2 V + \frac{(1-\tan^2\phi)}{a^2}V + \frac{2\sin\phi}{a^2\cos^2\phi}\frac{\partial U}{\partial\lambda}\right] + \frac{\partial\tau^y}{\partial z\rho_0} \\
&\frac{\partial P}{\partial z} = -\rho g \qquad \frac{1}{a\cos\phi}\frac{\partial U}{\partial\lambda} + \frac{1}{a\cos\phi}\frac{\partial}{\partial\phi}(V\cos\phi) + \frac{\partial W}{\partial z} = 0 \\
&\frac{\partial T}{\partial t} + L(T) = \frac{\partial}{\partial z}\left(\frac{K_v}{\Gamma}\frac{\partial T}{\partial z}\right) + K_h\nabla^2 T, \qquad \rho = \rho_0[1 - \alpha T(\lambda, \phi, z, t)], \qquad \alpha = 0.0002\ \text{deg}^{-1}
\end{aligned}\right\}, \quad \text{(A1)}$$

where

$$L(s) = \frac{1}{a\cos\phi}\frac{\partial}{\partial\lambda}(Us) + \frac{1}{a\cos\phi}\frac{\partial}{\partial\phi}(\cos\phi Vs) + \frac{\partial}{\partial z}(Ws)$$

and $f = 2\Omega\sin\phi$. Here ϕ, λ and z are the latitude, longitude and depth with corresponding velocities V, U, W; a is the radius of the earth and Ω its angular rotation speed. A linear equation of state which depends only on temperature has been used for simplicity and computational efficiency. Convective adjustment is included through the parameter Γ which is unity for $\partial\rho/\partial z > 0$ and zero for $\partial\rho/\partial z < 0$. The basin is 17° wide, extending from 23.5 to 50°N and is 2000 m deep. Continental shelf topography is included along the eastern boundary. The topography has a linear shelf and slope defined by (4.1).

The model has 15 grid points in the vertical. Horizontal velocity is evaluated at 10, 30, 50, 70, 90, 115, 145, 175, 205, 235, 275, 350, 500, 900 and 1600 m depths. The horizontal resolution is 0.08° in the zonal direction over the shelf increasing to 0.5° in the west.

The meridional resolution is 0.5° (0.14° for the small wind scale case). A horizontal viscous damping layer is included along the northern ($A_h \times 20$), western ($A_h \times 100$), and southern ($A_h \times 20$) boundaries in order to reduce the influence of these boundaries on the eastern basin response. Here $A_h = 5.0 \times 10^5$ cm^2 s^{-1} is the interior viscosity. The damping layer in the west is 3° wide.

Friction. The basic vertical diffusion and dissipation are Richardson Number dependent with the form

$$\left.\begin{aligned} A_v &= \frac{\nu_0}{(1 + \gamma\ \mathrm{Ri})^2} + \nu_b \\ K_v &= \frac{A_v}{(1 + \gamma\ \mathrm{Ri})^2} + K_b \end{aligned}\right\},$$

where $\mathrm{Ri} = \alpha g T_z/(U_z^2 + V_z^2)$. The base values ν_b and K_b used here are 0.0134 and 0.00134 cm^2 s^{-1}, $\gamma = 5.0$, and $\nu_0 = 50.0$ cm^2 s^{-1}. This parameterization of friction is similar to that proposed by Munk and Anderson (1948) and discussed by Hamilton and Rattray (1978). Pacanowski and Philander (1981) explore the parameter ranges of this form of friction in the context of the equatorial ocean.

The model also includes turbulent bottom dissipation where the vertical gradient of velocity at the bottom is

$$\left.\begin{aligned} A_v \frac{\partial U}{\partial z} &= C_D|\mathbf{U}|(U\cos\phi - V\sin\phi) \\ A_v \frac{\partial V}{\partial z} &= C_D|\mathbf{U}|(U\sin\phi + V\cos\phi) \end{aligned}\right\},$$

where $\phi = 10°$ is a frictional turning angle. This form of bottom friction is used extensively in atmospheric models, and has been used by Csanady (1976), for example, with $\phi = 0°$ in studying coastal circulation.

The equations of motion are integrated following the method of Bryan (1969). Taking the curl of the vertically averaged equations of motion, pressure is eliminated and a predictive equation for an integrated transport streamfunction is obtained. The internal mode velocity components are predicted from the vertical derivative of the momentum equation where the vertical gradient of the pressure is eliminated by the hydrostatic equation. In this way surface pressure does not explicitly enter the equations being integrated.

The streamfunction is uniform along horizontal boundaries. Vertical mixing occurs between adjacent boxes every 17th time step. The pressure and Coriolis terms are treated semi-implicitly for greater computational efficiency. This has the effect of reducing the amplitude of high frequency internal waves, but these waves are not of interest in this study. Further discussion of the computational scheme is given in Semtner (1974).

REFERENCES

Allen, J. S., 1973: Upwelling and coastal jets in a continuously stratified fluid. *J. Phys. Oceanogr.*, **3**, 245–257.

——, 1976: Some aspects of the forced wave response of stratified coastal regions. *J. Phys. Oceanogr.*, **6**, 113–119.

——, 1980: Models of wind-driven currents on the continental shelf. *Annual Reviews in Fluid Mechanics*, Vol. 12, Annual Reviews, 389–433.

Bryan, K., 1969: A numerical method for the study of the circulation of the world ocean. *J. Comput. Phys.*, **4**, 347–376.

Chao, S.-Y., 1981: Forced shelf circulation by an alongshore wind band. *J. Phys. Oceanogr.*, **11**, 1325–1333.

Charney, J. G., 1955: The generation of oceanic currents by wind. *J. Mar. Res.*, **14**, 477–498.

Crepón, M., and C. Richez, 1982: Transient upwelling generated by two-dimensional atmospheric forcing and variability in the coastline. *J. Phys. Oceanogr.*, **12**, 1437–1457.

Csanady, G. T., 1976: Mean circulation in shallow seas. *J. Geophys. Res.*, **81**, 5389–5399.

——, 1978: The arrested topographic wave. *J. Phys. Oceanogr.*, **8**, 47–62.

Gill, A. E., and A. J. Clarke, 1974: Wind-induced upwelling, coastal currents and sea-level changes. *Deep-Sea Res.*, **21**, 324–345.

——, and E. H. Schumann, 1974: The generation of long shelf waves by the wind. *J. Phys. Oceanogr.*, **4**, 83–90.

Hamilton, P., and M. Rattray, Jr., 1978: A numerical model of the depth-dependent wind-driven upwelling circulation on a continental shelf. *J. Phys. Oceanogr.*, **8**, 437–457.

Huthnance, J. M., 1978: On trapped waves: Analysis and numerical calculation by inverse iteration. *J. Phys. Oceanogr.*, **8**, 74–92.

Kundu, P. K., J. S. Allen and R. L. Smith, 1975: Modal decomposition of the velocity field near the Oregon coast. *J. Phys. Oceanogr.*, **5**, 683–704.

McCreary, J. P. Jr., 1981: A linear stratified ocean model of the coastal undercurrent. *Phil. Trans. Roy. Soc. London*, **302**, 385–413.

Mooers, C. N. K., C. A. Collins and R. L. Smith, 1976: The dynamic structure of the frontal zone in the coastal upwelling region off Oregon. *J. Phys. Oceanogr.*, **6**, 3–21.

Munk, W. H., and E. R. Anderson, 1948: A note on the theory of the thermocline. *J. Mar. Res.*, **1**, 276–295.

Pacanowski, R., and S. G. H. Philander, 1981: Parameterization of vertical mixing in numerical models of tropical oceans. *J. Phys. Oceanogr.*, **11**, 1443–1451.

Pedlosky, J., 1978: A nonlinear model of the onset of upwelling. *J. Phys. Oceanogr.*, **8**, 178–187.

Philander, S. G. H., and J.-H. Yoon, 1982: Eastern boundary currents and coastal upwelling. *J. Phys. Oceanogr.*, **12**, 862–879.

Semtner, A. J., Jr., 1974: An oceanic general circulation model with bottom topography. Tech. Rep. No. 9, Dept. of Meteor., University of California, Los Angeles, 99 pp.

Suginohara, N., 1982: Coastal upwelling: Onshore–offshore circulation, eastward coastal jet and poleward undercurrent over a continental shelf-slope. *J. Phys. Oceanogr.*, **12**, 272–284.

Yoon, J.-H., and S. G. H. Philander, 1982: The generation of coastal undercurrents. *J. Oceanogr. Soc. Japan*, **38**, 215–224.